X-ray transient absorption spectroscopy by ultrashort x-ray laser pulse in continuous-wave-IR field

Xin Shi,[1] Yong Wu,[2,3] Jian Guo Wang,[2] Victor Kimberg,[4,5,6,*] and Song Bin Zhang,[1,†]

[1]School of Physics and Information Technology, Shaanxi Normal University, Xi'an 710119, China

[2]Institute of Applied Physics and Computational Mathematics, Beijing 100088, China

[3]Center for Applied Physics and Technology, Peking University, Beijing 100084, China

[4]Theoretical Chemistry and Biology, Royal Institute of Technology, Stockholm 10691, Sweden

[5]Siberian Federal University, 660041 Krasnoyarsk, Russia

[6]Kirensky Institute of Physics, Federal Research Center KSC SB RAS, 660036 Krasnoyarsk, Russia

Abstract

X-ray transient absorption spectra (XTAS) of molecules are theoretically investigated in a femtosecond x-ray pump and continuous wave (CW) infrared (IR)-control scenario. The scheme is exemplified by CO molecule resonantly pumped into carbon and oxygen core-excited $1s\rightarrow\pi^*$ states by a weak femtosecond x-ray pulse, while dynamic Stark shifts are induced by the CW IR-control radiation. As a result, significant shoulder structures appear in XTAS showing strong dependence on the phase of IR radiation relative to the envelope of the x-ray pulse. Due to a significant difference in the frequencies of the two pulses, the present XTAS scheme provides much clear interpretation of the dynamic Stark effects as compared to attosecond UV transient absorption scenario. Within suggested two-level model, where the total spectrum is decomposed as incoherent superposition of contributions from different vibrational excitations weighted by the Frank-Condon Factors, all spectral structures can be well identified and interpreted in a good agreement with the full-scale molecular simulations. Well characterized XTAS in the proposed IR-control scheme can be applied for fine phase synchronization between IR and x-ray pulses, highly demanded in the modern experiments at x-ray free-electron lasers.

PACS: 32.30.Rj, 32.80.Hd, 33.20.Xx

* kimberg@kth.se

† song-bin.zhang@snnu.edu.cn

Key Words: transient absorption spectra, ultrashort x-ray pulse, nuclear wavepacket dynamics, dynamic Stark shift

I. Introduction

In the past decades of attosecond science [1-4], attosecond transient absorption spectroscopy (ATAS) has become a general versatile tool to investigate the electronic and nuclear dynamics of atomic and molecular systems [5-20]. In the scenario of ATAS, the system pumped by a femtosecond IR field is probed by measuring the absorption spectrum of the time delayed attosecond ultraviolet (UV) pulse, the spectral shape exhibiting emission and absorption is precisely manipulated by the relative phase between the two pulses through fine variation of the time delay [21]. Well-known applications of ATAS include manipulating auto ionization state of Argon [13] and doubly excited state of Helium [10], emerging the signature of conical intersections [5] and the attosecond band-gap dynamics of silicon [22], as well as many others [8,12,19,23,24].

Recently, the technique of ATAS has been extended into x-ray region to investigate the inner shell dynamics of molecules pumped by femtosecond x-ray pulses [25-28]. Thanks to the advanced development of x-ray free-electron laser (XFEL) facilities [29-31] and tabletop attosecond sources [32-34], ultrashort x-ray pulses with pulse duration down to femtosecond and even sub-femtosecond range are experimentally achievable [28,35-37], x-ray transient absorption spectra (XTAS) shed light on inner shell wave packet dynamics, complemented with the Auger electron spectroscopy by ultrashort x-ray pulses [25,38,39]. Due to high spatial localization of core-orbitals addressed by x-ray, XTAS becomes a unique element and sight specific spectroscopic tool, contrary to ATAS where a delocalized valence excitation is employed. Note that recent femtosecond transient absorption experiments on carbon K-edge of CF_4 [26] and 1,3-cyclohexadiene [27] were mainly focused on the slow nuclear-rearrangement dynamics, and hence did not strongly rely on the ultrashort time resolution of the x-ray pulses. Similar applications for slow chemical reaction processes have been proposed and investigated by ultrashort x-ray pulses in chemical physics [40,41]. However, XTAS has a great potential to imprint ultrafast physical processes such as Auger decay, as it was shown in transient absorption experiments at argon $L_{2,3}$ edge (~250 eV), which has been successfully performed by

sub-femtosecond x-ray pulse in the presence of an infrared (IR) control pulse [28]. Theoretically, investigation of the nonlinear nuclear dynamics of core-excited CO molecule, using femtosecond x-ray pump and strong x-ray control scenario [25], has clearly shown that XTAS depend dramatically on varying the time delay between the two pulses allowing to retrieve the nonlinear nuclear wave packet dynamics.

In the present paper we consider XTAS of molecules employing femtosecond x-ray pump and continuous wave (CW) IR-control pulses. The studied XTAS scheme provides much simpler interpretation, as compared to ATAS technique. Indeed, due to large difference between IR and x-ray frequencies, the couplings between the control and pump fields are negligibly small, which allows for clear observation of the IR-induced effects in the x-ray absorption spectra and to neglect the IR contribution on the x-ray transitions. Moreover, many cycle oscillations of the x-ray field during the pulse duration allow to neglect the carrier-envelope phase (CEP) effect, and the dependence of IR phase is measured relative to intensity peak of the x-ray pulse. Theoretically, it makes the rotating wave approximation (RWA) for x-ray radiation a robust technique, as it was shown previously [25]. Using pre-aligned CO molecule as a prototype, CO is resonantly pumped by a weak femtosecond x-ray pulse from the 'initial' (*I*) ground $\left|\mathrm{X}\ ^1\Sigma^+\right\rangle_I$, to the carbon (oxygen) K-edge core-excited 'final' (*F*) state $\left|\mathrm{C}1s^{-1}\pi^*\ ^1\Pi\right\rangle_F$ ($\left|\mathrm{O}1s^{-1}\pi^*\ ^1\Pi\right\rangle_F$) (see Fig. 1); simultaneous dynamic Stark shifts induced by the IR-control radiation on both ground and core-excited states are also taken into consideration. It is found that the dynamic Stark effect is exhibited as significant shoulder structures in XTAS, and these XTAS structures can be efficiently manipulated by varying the time delay or, equivalently, the IR phase–relative to the peak of the x-ray pulse envelope. These shoulder structures were observed previously in ATAS for a polar molecule [16], where the absorption to a dissociative valence excited state is considered. In the present case however, we consider excitation to the bound core-excited state with a discrete vibrational spectrum, which allows to considerably simplify the physical picture of the dynamic Stark effect separating the contributions from different vibrational levels in the core-excited state. This, together with other advantages of XTAS discussed above, allowed to use a simplified two-level model to predict the behavior of the full molecular system with good accuracy. In the constructed two-level model system for levels $\left|0\right\rangle_{\mathrm{I}}$ and $\left|\nu_0\right\rangle_{\mathrm{F}}$ of the ground and core-excited states,

respectively, the total XTAS spectra can be efficiently decomposed as incoherent sum of different vibrational contributions weighted by the Frank-Condon factors and thus most important spectral features can be well identified and interpreted. The observed effect of the phase dependent XTAS shoulder structures can be used to solve an inverse problem of the fine phase synchronization of the ultrashort x-ray pulse to the 'comb' of the CW IR radiation using experimental XTAS, an important task in many modern XFEL applications. The generalization of the present scenario and theoretical analysis to more complex systems are also possible, as it is outlined in the paper.

The paper is organized as follows. The numerical methods for diatomic molecule are briefly introduced in the Section II; the simplified two-level model and its approximate analytical solution is presented in Section II A and II B, respectively; the details of the numerical simulations are summarized in Section II C. Section III is devoted to discussions of the numerical results for the two-level model (III A) and a real molecule at carbon K- (III C) and oxygen K- (III D) edges; scheme for possible experimental phase synchronization is also proposed and discussed (III B). Summary of our findings are collected in Section IV. Unless otherwise stated, atomic units (a.u.) are used throughout the paper.

II. Theoretical methods

The theory of transient absorption spectra has been comprehensively presented in Refs. [21,42,43], here we will briefly summarize it. The intensities of the transient absorption spectra are proportional to the response function $S(\omega)$, representing the absorption probability cross-section at a given frequency ω, defined as [21]

$$S(\omega) = -2\,\mathrm{Im}[d(\omega)E^*(\omega)], \tag{1}$$

where $d(\omega)$ and $E(\omega)$ are the Fourier transforms of the time-dependent induced transition dipole moment $d(t) = \langle \Psi(t) | \hat{d} | \Psi(t) \rangle$ and the electric field $E(t)$, respectively. In what follows we study absorption and emission of the x-ray radiation by the pre-aligned ensemble of diatomic molecules with their transition dipole moment parallel to the polarization vector of the x-ray field. $|\Psi(t)\rangle$ is the total time dependent wave function of the system in the electric field. For the quasi-resonant interaction with x-ray laser pulse studied here (see Fig. 1), the wave function

involved in the absorption process can be well expanded by the ground one $|\phi_I\rangle$ and the resonant core-excited one $|\phi_F\rangle$ within the frame of Born-Oppenheimer approximation as [39,44]

$$|\Psi(q,t)\rangle = c_I(q,t)|\phi_I\rangle + c_F(q,t)|\phi_F\rangle, \tag{2}$$

where q represents the nuclear degrees of freedom, $c_I(q,t)$ and $c_F(q,t)$ are corresponding time dependent expansion coefficients for the electronic states $|\phi_I\rangle$ and $|\phi_F\rangle$, respectively. The nuclear Hamiltonian of the system can be written as [39,44]

$$H(R,t,t_0,\varphi) = -\frac{1}{2\mu}\frac{\partial^2}{\partial R^2}\mathbf{I} + \begin{pmatrix} V_I(R) & D^{\dagger}(\omega_{xfel},t,t_0) \\ D(\omega_{xfel},t,t_0) & V_F(R) - \frac{i}{2}\Gamma_F \end{pmatrix}, \tag{3}$$

where the first term describes the kinetic energy of the nuclear motion with μ and R are the reduced mass and internuclear distance, respectively; and the second term includes the potential energy curve $V_X(R)$ of electronic state $|\phi_X\rangle$ $(X = I, F)$, Γ_F is the decay rate of the core-excited state. Off-diagonal terms of the Hamiltonian in Eq. (3) describe quasi-resonant interaction with the weak x-ray pulse. Supposing the electronic transition dipole moment $d_{IF} = \langle\phi_I|\hat{d}|\phi_F\rangle$ is not sensitive to the internuclear distance, we can define the dipole coupling matrix element $D(\omega_{xfel},t,t_0)$=$d_{IF}g_0 g(t,t_0)\cos(\omega_{xfel}(t-t_0))$ induced by the x-ray pulse with electric field intensity, envelope and central frequency being g_0, $g(t,t_0) = e^{-(t-t_0)^2/\tau^2}$ and ω_{xfel}, respectively.

In the presence of strong CW IR control field the Hamiltonian of the system should be modified by including the additional dynamic Stark shift of the ground and core-excited electronic states as:

$$\tilde{H}(R,t,t_0,\varphi_{IR}) = -\frac{1}{2\mu}\frac{\partial^2}{\partial R^2}\mathbf{I} + \begin{pmatrix} V_I(R) - d_I\varepsilon_{IR}(t,t_0,\varphi_{IR}) & D^{\dagger}(\omega_{xfel},t,t_0) \\ D(\omega_{xfel},t,t_0) & V_F(R) - d_F\varepsilon_{IR}(t,t_0,\varphi_{IR}) - \frac{i}{2}\Gamma_F \end{pmatrix}, \tag{4}$$

where the IR electric field $\varepsilon_{IR} = \varepsilon_0\cos[\omega_{IR}(t-t_0)+\varphi_{IR}]$ with amplitude ε_0 is aligned parallel to the permanent dipole moments of the molecule in the ground and core-excited states, d_F and d_I, respectively. We neglect the IR field contribution to the off-diagonal terms in Eq. (4), which is a reasonable approximation due to a very large energy difference between the IR field frequency and x-ray transitions considered in our study. In the case of UV ATAS, the effect of IR field

contribution to the off-diagonal elements can be observed as formation of 'ladder structure' [16] with energies equals to the multiple of IR photon energy $n\omega_{IR}$, $n = 2,3,\ldots$. The XTAS window, however, covers much higher energy range (near 300 eV in our case), which corresponds to an order of $1000\,\omega_{IR}$ (with ω_{IR}=0.3 eV). Such high order multiphoton process has negligibly small contribution to the electronic excitation. The Hamiltonian of Eq. (4) defines fully the evolution of the expansion coefficients in Eq. (2) with the solution of the following time-dependent Schrödinger equation:

$$i\frac{\partial}{\partial t}\begin{pmatrix} c_I(R,t) \\ c_F(R,t) \end{pmatrix} = \tilde{H}(R,t,t_0,\varphi_{IR})\begin{pmatrix} c_I(R,t) \\ c_F(R,t) \end{pmatrix}. \tag{5}$$

With the molecule initially populated at its ground vibrational state $|0\rangle_I$, Eq. (5) can be fully solved and the transient absorption spectra can be computed using Eqs. (1-2). It is worth noting, that only difference in the dynamic Stark shift for the two electronic states, defined as

$$\Delta s_{IR}(t,t_0,\varphi_{IR}) = \Delta\Omega_{IR}\cos[\omega_{IR}(t-t_0)+\varphi_{IR}], \tag{6}$$

is observable in XTAS; here $\Delta\Omega_{IR} = \varepsilon_0(d_F - d_I)$ is the difference Rabi frequency of CW IR field arising from difference in the values of permanent dipole moment of the ground and core-excited states. Due to this, the Hamiltonian of Eq. (4) can be written in an alternative form using Eq. (6) as

$$\tilde{H}(R,t,t_0,\varphi_{IR}) = -\frac{1}{2\mu}\frac{\partial^2}{\partial R^2}\mathbf{I} + \begin{pmatrix} V_I(R) & D^{\dagger}(\omega_{xfel},t,t_0) \\ D(\omega_{xfel},t,t_0) & V_F(R) - \Delta S_{IR}(t,t_0,\varphi_{IR}) - \frac{i}{2}\Gamma_F \end{pmatrix}, \tag{7}$$

which is used in the simulation performed in the present study.

II A. Two-level model

The conventional x-ray absorption spectrum of CO at carbon K-edge consists of three well resolved vibrational peaks [45]. Tuning the frequency of the weak x-ray pump, different vibrational states of the core-excited electronic state $|\phi_F\rangle$ can be excited independently with the amplitude defined by the value of the corresponding transition dipole moment and the x-ray pulse frequency detuning from the resonance. Taking this into account, the expansion coefficients of Eq. (2) used for the solution of Eq. (5) could be approximated as:

$$\begin{aligned} c_I(R,t) &\simeq c_0^I(t)|0\rangle_I \\ c_F(R,t) &= \sum_v w_{0v}^{IF} c_v^F(t) e^{-i\Delta E_{v0}^{FI}t}|v\rangle_F \end{aligned}, \tag{8}$$

where $|0\rangle_I$ and $|v\rangle_F$ are the vibrational eigenfuctions of the ground and core-excited states,

respectively, and ΔE_{v0}^{FI} is the energy difference between them; $w_{0v}^{IF} = {}_I\langle 0|v\rangle_F$ is the overlap integral between the two vibrational states, its module square corresponds to the Frank-Condon factor $f_{0v}^{IF} = \left|w_{0v}^{IF}\right|^2$. Introducing Eq. (8) into Eq. (5) the R-dependence vanishes, and the problem is reduced to a set of the following simplified two-level model equations (see Fig. 1c) for R-independent expansion coefficients as

$$i\frac{\partial}{\partial t}\begin{pmatrix} c_0^I(t) \\ c_v^F(t)e^{-i\Delta E_{v0}^{FI}t} \end{pmatrix} = \begin{pmatrix} 0 & D(\omega_{xfel},t,t_0) \\ D(\omega_{xfel},t,t_0) & \Delta E_{v0}^{FI} - \Delta s_{IR}(t,t_0,\varphi_{IR}) - \frac{i}{2}\Gamma_F \end{pmatrix}\begin{pmatrix} c_0^I(t) \\ c_v^F(t)e^{-i\Delta E_{v0}^{FI}t} \end{pmatrix}. \tag{9}$$

Note that within the weak field limit $c_0^I(t) \simeq 1$ and the total induced dipole moment $d(t)$ could be approximated as

$$\begin{aligned} d(t) &\simeq \sum_v f_{0v}^{IF} d_{0v}^{IF}(t) \\ d_{0v}^{IF}(t) &= 2d_{IF}\,\mathrm{Re}\left[c_v^F(t)e^{-i\Delta E_{v0}^{FI}t}\right] \end{aligned}, \tag{10}$$

where the summation is taken over all vibrational levels of the core-excited state with sufficient contribution to the x-ray absorption cross section. Here $d(t)$ is expressed as incoherent sum of the time-dependent induced dipole moments for each vibrational level in the core-excited state $d_{0v}^{IF}(t)$ weighted by the Frank-Condon factor f_{0v}^{IF}. The evolution of the induced dipole moment is defined by the evolution of the core-excited wave packet $c_v^F(t)\, e^{-i\Delta E_{v0}^{FI}t}$ multiplied by the transition dipole moment (d_{IF}) between the ground and core-excited electronic states. The two-level approximation introduced above neglects the lifetime vibrational interference (LVI) in the core-excited state, which is shown to be rather small for the excitation of CO molecule at carbon K-edge due to rather large vibrational energy difference of about 0.3 eV, as compared to the lifetime broadening of 0.08 eV at carbon K-edge [45]. This effect is however significant at Oxygen K-edge absorption, as discussed below (Sec. III D).

To compute the XTAS cross section of Eq. (1), we need to compute the Fourier transform of the induced transition dipole moment from Eq. (10) as $d(\omega) = \sum_v f_{0v}^{IF} d_{0v}^{IF}(\omega)$, here $d_{0v}^{IF}(\omega)$ is the Fourier transforms of $d_{0v}^{IF}(t)$. The time dependence of the core-excited wave packet has contribution from $c_v^F(t)$ and $e^{-i\Delta E_{v0}^{FI}t}$ terms, with low and high frequencies, respectively. Due to

this the central frequency of the Fourier transform $d_{0v}^{IF}(\omega)$ will be located around the resonant energy ΔE_{v0}^{FI}, with some shoulder structures correspondent to the $c_v^F(t)$ frequency component. Finally, the XTAS profile for a molecular system interacting with the weak x-ray pump field could be approximated as a superposition of the XTAS profiles for two-level systems $S_{0v}(\omega) = -2\,\mathrm{Im}[d_{0v}(\omega)E^*(\omega)]$ computed for each core-excited vibrational level separately as

$$S(\omega) \simeq \sum_v f_{0v}^{IF} S_{0v}(\omega)\,. \tag{11}$$

The present model allows to avoid the complex solution of the nuclear dynamic equations for molecules of Eqs. (1-5) using sufficiently cheaper numerical simulation schemes when all vibrational contributions can be computed independently in a parallelized algorithm. Moreover, the proposed two-level model helps to distinguish the dynamic Stark effect from the nuclear dynamics targeting its physical meaning clearly. Fitting the theoretical spectrum of the two-level system to the experimental XTAS profile can also help to extract the parameters of the IR pulse (see Sec. III B) as well as some molecular constants. The theoretical-experimental fitting of the solution of the full molecular system of Eq. (5) is quite complex and thus impractical in real implementation. In Sec. III A we will analyze the behavior of the two-level system and corresponding XTAS properties with respect to variation of the pump frequency detuning from the resonance $\Delta = \Delta E_{v0}^{FI} - \omega_{xfel}$, decay rate of the core-excited state Γ_F, IR pulse intensity $\Delta\Omega_{IR}$ and frequency ω_{IR}, as well as the phase φ_{IR} of the IR field.

II B. Analytical solutions for the two-level model

The simplified two-level model, discussed above, can also be solved analytically with some reasonable approximations. Making use of the rotating wave approximation for x-ray field by neglecting the fast oscillating terms $\sim e^{i(\Delta E_{v0}^{FI} + \omega_{xfel})t}$ in Eq. (9) we can write the expression for the core-excited wave packet $c_v^F(t)$ as

$$\frac{dc_v^F(t)}{dt} + c_v^F(t)\left(\frac{\Gamma_F}{2} - i\Delta s_{IR}(t,t_0,\varphi_{IR})\right) = -\frac{i}{2}\Omega_{IF}\, e^{i\Delta t}\, g(t,t_0). \tag{12}$$

Here we assumed that the weak x-ray field does not create any sufficient change of the population of the ground state, so that $c_0^I(t) \approx c_0^I(0) = 1$; $\Omega_{IF} = d_{IF} g_0$ is Rabi frequency of the field on x-ray transition. Let us consider the case of resonant excitation $\Delta = 0$ by the pump x-ray pulse with the

duration much shorter as compared to the other characteristic times of the system $\tau \ll 1/\Gamma_f, 2\pi/\omega_{IR}, t_0$. In that case the Gaussian function can be approximated by the delta function $g(t,t_0) \approx \delta(t-t_0)$ allowing for easy integration of Eq. (12). Our analysis of the numerical solution has shown that for the parameters discussed in the present paper this is a reasonable approximation, while for $\tau \le 0.5$ fs this condition is fully satisfied. For $t \ge t_0$, the induced wave packet reads:

$$c_v^F(t) = -\frac{i}{2}\Omega_{IF}\, e^{\Gamma_f (t_0 - t)/2} \exp\left\{ i\kappa \left[\sin\left(\omega_{IR}(t-t_0) + \varphi_{IR}\right) - \sin\varphi_{IR} \right] \right\}, \tag{13}$$

where the ratio $\kappa = \Delta\Omega_{IR}/\omega_{IR}$ describes the intensity and frequency of IR-induced effects. With the help of Eq. (13), we can get the induced dipole moment of Eq. (10) in the time-domain as

$$d_{0v}^{IF}(t) = d_{IF}\Omega_{IF}\, e^{\Gamma_f (t_0 - t)/2} \sin\{\Delta E_{v0}^{FI} t - \kappa \sin[\omega_{IR}(t-t_0) + \varphi_{IR}] + \kappa \sin\varphi_{IR}\}. \tag{14}$$

The structure of the above equation is quite clear. The first term $d_{IF}\Omega_{IF}$ describes the amplitude of the core-excitation process. The second, time-dependent, term describes non-radiative decay of the core-excited state by Auger process with the time-scale Γ_f, resulting in a lifetime broadening of all spectral resonances. The third, periodic, term describes all resonances in XTAS appearing in the present model. The first term under sin-function corresponds to the main peak in the frequency domain, that is $|0\rangle_I \to |\nu\rangle_F$ core-excitation transition of energy ΔE_{v0}^{FI}. The second term under sin-function describes the effects of the IR field; obviously, it vanishes when the IR field is off ($\kappa = 0$). This term shows periodic behavior with the frequency of IR field ω_{IR} and its relative value is proportional to the IR field intensity and inverse proportional to the IR frequency. Moreover, the amplitude of the IR-term is also affected by the IR phase through the constant '$\kappa \sin\varphi_{IR}$'. Note that numerical Fourier transformation of analytical solution of Eq. (14) nearly coincide with the full numerical solution of the two-level model of Eq. (9) at the range of parameters, discussed in detail in Sec. III A. The Fourier transform of the XFEL field $E(\omega)$ defines a spectral window of XTAS (Eqs. (1, 12)). For derivation of Eq. (14), we supposed an extremely short XFEL pulse corresponding to the broad-band spectral function $E(\omega)$.

II C. Simulation details

In the following Section III, the XTAS simulation for the two-level model will be studied and compared to the full solution for the CO molecule. In the simulation we use an ultrashort x-ray

pump laser pulse (τ =2 fs) with its electric field polarization vector parallel to the molecular transition dipole moment and the central frequency $\omega_{xfel} \simeq \Delta E_{00}^{FI}$ =287.4 eV (533.4 eV), resonant to the lowest vibrational level of the carbon (oxygen) $1s \rightarrow 2\pi^*$ core-excited state of CO, respectively. The Rabi frequency of the x-ray field on the resonant transition is chosen to be sufficiently weak $\Omega_{IF} = d_{IF} g_0$ =10^{-4} a.u. to avoid any nonlinear effects. Due to large x-ray frequency and quasi-resonant conditions the rotating wave approximation was used for description of the interaction of the x-ray pulse with molecular system. The core-excited state decay rate Γ_F =0.08 eV (decay lifetime of $1/\Gamma_F$ =8.2 fs) and Γ_F =0.18 eV [39] were used for the carbon K- and oxygen K- edges, respectively. The potential energy curves of the ground and core-excited states are modeled with Morse function using spectroscopic constants from Ref. [45]. The polarization of CW IR pulse is chosen parallel to the permanent dipole moment of the molecule and its period $T_{IR} = 2\pi / \omega_{IR}$ is much longer than the ultrashort x-ray pump pulse duration τ =2 fs. As we will show, the XTAS depends strongly on the dynamic Stark shift $\Delta s_{IR}(t, t_0, \varphi_{IR})$ and the relative phase φ_{IR} of the IR pulse with respect to the x-ray pulse envelope. In what follows, we used IR field with typical frequency $\omega_{IR} < 0.5$ eV ($T_{IR} > 8$ fs) and a moderate Rabi frequency of $\Delta\Omega_{IR} \simeq 0.1 \cdots 0.3$ eV. In the present study we focus on the dynamic Stark effects and avoid using larger IR intensities, when additional contribution from multiphoton processes becomes strong. The permanent dipole moments of the CO ground and core-excited states are about 0.04 and 0.3 a.u., respectively, resulting in the peak intensity of the IR field about 10^{14} W/cm^2, which is experimentally achievable [46,47]. The weak dependence of the permanent molecular dipole moment and transition dipole moment on the internuclear distance is neglected in the present study. The time dependent propagations of Eq. (5) are solved by the multi-configurational time-dependent Hartree (MCTDH) [25,48,49] method.

III. Results and Discussions

III A. Analysis of the two-level model

Let us start with the comprehensive analysis of the XTAS of the two-level system, before presenting the numerical results for CO molecule. The following typical set of parameters for the ultrashort x-ray pump pulse, the core-excited state and CW IR laser are chosen: $\Delta = 0$ (ω_{xfel}

=287.4 eV), Γ_F =0.1 eV, $\Delta\Omega_{IR}$ =0.1 eV, ω_{IR} =0.3 eV and φ_{IR} =0. The XTAS of the two-level system with respect to variation of these parameters are summarized in Figs. 2-6. Note that the central frequency ω_{xfel} is fixed and tuned to resonance with the lowest vibrational level $|0\rangle_F$ of the core-excited state; cases of $\Delta \neq 0$ correspond to the off-resonant excitation to the higher vibrational states $|v\rangle_F$ in a molecule by the broad bandwidth of the ultrashort pump pulse. In the present subsection we analyze behavior of the numerical solution of Eqs. (9-11), however the main features can be fully understood from the discussion of the analytical solution of Eqs. (13-14), employing the sudden pump approximation.

Fig. 2a shows the XTAS as a function of the relative photon energy $\Delta\omega = \omega - \omega_{xfel}$ for the x-ray pump with detuning Δ varying from -0.4 eV to 0.4 eV. The absorption spectra without CW IR pulse presented in the plot Fig. 2b, clearly shows a single absorption peak located at the resonance $\omega = E_{00}^{FI}$, equivalent to $\Delta\omega = \Delta$. The peak profile has an asymmetric shape typical for XTAS of the system with a fast decay channel [25] and its intensity reduces in the off-resonant pump cases following the Lorentzian resonance denominator. Turning on the strong CW IR field (Fig. 2a) does not change the character of the main spectral peak resulting from the x-ray pump field absorption, but it develops additional red and blue shifted shoulder structures due to dynamic Stark shift of the resonance according to the $c_v^F(t)$ evolution, perturbed by the IR field, see Eqs. (9,13). The effect of the IR field consists of absorption feature in the left spectral shoulder and symmetric emission feature in the right spectral shoulder of the main absorption resonance. The positions of these additional structures are determined by the frequency of IR radiation, as it will be discussed in detail below. Similar features were also predicted in the ATAS of LiF in XUV region [50]. The main difference of the present scheme from the one considered in Ref. [50] is a very large difference in the pump and IR frequencies $\omega_{xfel} / \omega_{IR} \sim 10^4$ (this relation equals to 5 in the ATAS case [50]), which makes all contribution from the multiphoton IR excitation negligibly small, providing clear signatures of the dynamic Stark effect that is the main topic of our paper. Moreover, in the present study the phase of IR field is defined relatively to the maximum of the XFEL pump pulse envelope. The pump pulse duration contents hundreds of the x-ray field cycles, allowing to neglect the CEP effect of XFEL pulse, which is very difficult to define in experiment.

The XTAS profiles for the decay width Γ_F varied from 0.05 eV to 0.3 eV are shown in Fig. 3 for the resonant pump excitation Δ=0, where the cases of IR field with $\Delta\Omega_{IR}$=0.1 & 0.2 eV, ω_{IR} =0.3 eV and φ_{IR}=0 (Figs. 3a, 3b) are compared against the case without IR radiation (Fig. 3c). Similar to Fig. 2, the spectra are featured by the dominant absorption peak of the x-ray pump pulse, while the IR field rises the shoulder structures, whose energy positions are not sensitive to the IR intensity in the present intensity range. Increase of the decay width Γ_F shortens the lifetime of the core-excited state so that the dynamics in this state become less and less significant, resulting in a gradual smearing out of the spectral features. The top of the main absorption peak is slightly shifted from $\Delta\omega$=0 due to the interference between the 'bound' and 'continuum' channels interpreted in Fano's model of resonance [51-53]. The hypothetical increase of the lifetime broadening discussed here illustrates the XTAS formation for the cases when core-excitation of other elements and edges are involved (e.g. Γ_F=0.05 eV corresponds to L-edge of *S*, Γ_F=0.30 eV corresponds to K-edge of *Na* [54], etc.). It is worth noting, that the intensity of the IR field does not change the energy position of the induced shoulder structures, but just affect their relative intensity (Figs. 3a, 3b) in full agreement with Eq. (14), where increase of parameter $\kappa = \Delta\Omega_{IR} / \omega_{IR}$ results in a larger relative contribution of IR field effect not changing its oscillation frequency.

Fig. 4 shows the XTAS (panel a) and the real part of the wave packet $\mathrm{Re}\left[c_v^F(t)\right]$ (panel b) with variation of the IR field frequency ω_{IR} from 0.1 eV to 0.5 eV; the other parameters are Δ =0, Γ_F=0.1 eV, $\Delta\Omega_{IR}$=0.1 eV and φ_{IR}=0. All spectra show the main absorption peaks (resulting from x-ray pump field absorption) of the same character near $\Delta\omega$=0, while the shoulder structures (absorption peak and emission valley), appearing due to the effect of the IR field, vary strongly depending on the IR frequency. Fig. 4a shows clearly that, the values of energy shifts between the main absorption peak and the shoulder structures are the multiples of the value of the IR frequency, related to the dynamic Stark shift (Eq. (6)), modulating the energy of the electronic states with the frequency ω_{IR}. Indeed, for ω_{IR}=0.1 eV one can see clearly IR-induced structures at $\Delta\omega = \pm 0.1$ and ± 0.2 eV. For the larger IR frequencies (0.3 eV and higher) we can observe only one symmetric XTAS shoulder structure at $\Delta\omega = \pm\Delta\omega_{IR}$, since at larger relative photon energies the XTAS cross section becomes small due to a limited bandwidth of the used x-ray pump pulse

(~1eV).

The formation of the shoulder spectral structures is fully defined by the dynamics of the induced core-excited wave packet, shown in Fig. 4b. Indeed, the XTAS profile is defined by the Fourier transform of the induced dipole moment of Eq. (10), so the absorption or emission character of the spectral features (peak or valley) results from the interference between the dominant absorption peak contribution and the induced wave packet $c_v^F(t)$ (see Eqs. (13-14)), which is fully characterized by the intensity, frequency and phase of the IR field. With the parameters used in Fig. 4 for all IR frequencies, the first left and first right shoulder structures have character of peak and valley, respectively, corresponding to the constructive and destructive interference. As we will see below, the variation of IR phase φ_{IR} changes the interference character drastically. Variation of ω_{IR} changes both the position and shape of the shoulder structures. For the weak IR field approximation $\kappa \ll 1$, the oscillating term of the real part of the wave packet reads

$$\mathrm{Re}\left[c_v^F(t)\right] \propto \kappa \sin\left[\omega_{IR}(t-t_0)+\varphi_{IR}\right]-\kappa\sin\varphi_{IR}, \qquad (15)$$

where one can see the double effects of ω_{IR}: (1) change the period of oscillation or corresponding frequency shift of the IR-inducer shoulder structures in XTAS; (2) change the amplitude of the IR-induced oscillations of the wave packet (Fig. 4b) via parameter $\kappa = \Delta\Omega_{IR}/\omega_{IR}$. This explains why the intensity of the shoulder structures increase with decreasing of ω_{IR} at the same value of $\Delta\Omega_{IR}$ (Fig. 4a). The exponential decay term with Γ_F =0.1 eV in Eqs. (13-14) results in the fast attenuation of the wave packet amplitude (Fig. 4b), limiting the observation time and thus the sharpness of the spectral structures.

Figs. 5-6 show details of the XTAS with respect to the changes of the relative phase φ_{IR}; the other parameters chosen as Δ =0, Γ_F =0.1 eV, $\Delta\Omega_{IR}$ =0.1 eV, and ω_{IR} =0.3 eV. The most significant feature exhibited in Fig. 5 is the periodic variation of the shoulder structures with changing of φ_{IR} from 0 to 2π, where the left and right shoulder structures experience the evolutions peak-valley-peak and valley-peak-valley, respectively. The dashed line at $\Delta\omega = -0.29$ eV corresponds to the maximal change in the XTAS intensity with the phase change and will be analyzed in the following subsection in connection to the technique of synchronization of the IR envelope with XFEL pulse. Fig. 6 presents the results for six specific values of φ_{IR} together with

the corresponding evolutions of $\mathrm{Re}\left[c_0^F(t)\right]$, allowing for better understanding of the XTAS formation. Fig. 6a clearly shows the evolutions of the shoulder structures with respect to the relative phase φ_{IR}, which correlates fully with the evolutions of $\mathrm{Re}\left[c_0^F(t)\right]$ induced by the IR field (Fig. 6b). As it was already discussed above, the absorption or emission character of the IR-induced shoulder structures is defined by the interference between the wave packet term and the main x-ray absorption term, and thus can be fully controlled by controlling the phase of the IR field (Fig. 6a). Note that in the case of $\Delta \neq 0$ (not shown here), the XTAS possess quite similar features as for the case of $\Delta = 0$. Variation of φ_{IR} only changes the shape of the shoulder structure but not its position. One can also see small change of the peak position of the main absorption resonance (Figs. 5-6a), which can be explained by its overlap with the shoulder structures.

III B. Mapping the IR field profile using dynamic Stark shift in XTAS

Recent development of XFEL facilities opens new possibilities for various IR-pump x-ray-probe techniques [55-57], where an accurate synchronization of the x-ray pulse on the IR electric field profile is of crucial importance. The dynamic Stark effect studied here within the XTAS scheme can be considered as a promising tool for fine synchronization of the IR field 'comb' with the ultrashort x-ray pulse. The proposed realization is based on our observation of the strong phase-dependence of the IR-induced shoulder structure. Indeed, the cut of the 2D XTAS map (Fig. 5, dashed line) at the maximum of the left shoulder structure $S(\varphi_{IR})$ at $\Delta\omega = -0.29\,\mathrm{eV}$ is a periodic function of the phase φ_{IR} (Fig. 7a), which mimics the profile of $E_{IR}(t)$ with period $T_{IR} = 2\pi / \omega_{IR}$ plotted in the Fig. 7b. Apparently, the change of IR phase φ_{IR} relative to the peak of x-ray pulse is fully equivalent to the change of the x-ray peak position ('observation time' t_0) relatively to the 'comb' of IR field. Indeed, one can express the total phase of the oscillating term in Eq. (15) as $\varphi = \varphi_{IR} - \omega_{IR} t_0$, which can be altered by variation of either φ_{IR} or t_0.

The experimental realization of the proposed synchronization scheme is based on the use of several sequential x-ray pulses at times $t = t_0, t_1, t_2 \ldots$ during the coherence time of the IR pulse (see Figs. 7a,b). The periodic IR field $\varepsilon_{IR}(t) \sim \cos(\omega_{IR} t)$ induces periodic dynamics of the core-excited wave packet with frequency ω_{IR} and relative phase shift of π via the dynamics Stark shift (Eqs. (13-15)). The wave packet dynamics is probed by sequential x-ray pulses in

XTAS scheme as it is illustrated in Fig. 7b. Let us first consider the case, when x-ray pulse at t_0 coincides with the maximum of the $\varepsilon_{IR}(t)$ envelop, $\varphi_{IR}=0$ (Fig. 7b), resulting in the maximum of XTAS shoulder structure (Fig. 7a). This first measurement at t_0 is used as the reference point. The second x-ray pulse at time t_1 probes another point of the wave packet oscillatory profile corresponding to relative phase $\varphi=\omega_{IR}(t_1-t_0)$. The delay time can be chosen in a way that it probes the wave packet (and thus IR field envelope) at different phase shifts, equivalent to introducing $\varphi_{IR}=\omega_{IR}t_d$ (d=0, 1, 2…). Measurements of the XTAS shoulder structure at several delay times t_d (Fig. 7a) allows to reconstruct the IR field envelope and to perform an accurate phase synchronization with x-ray facility.

Measurements, in principle, can be performed with the delay time longer than the period of IR field $\Delta t=t_d-t_0>T_{IR}$, however, shorter than the IR pulse coherence time (with a good precision $\delta(\Delta t)<<T_{IR}$) is required to achieve high level phase synchronization. Another limiting factor for the method's accuracy is the short core-excited lifetime $1/\Gamma_F$ (~10 fs). It results in the fast decay of the wave packet amplitude (Fig. 6b, 7b), which reduces the 'observation' time and thus increases the broadening of XTAS structures (Fig. 3). As one can see from Fig. 5, the phase-dependence of the IR-induced *left* and *right* shoulder structures have the same period (experience the phase shifts about π). The use of the *right* shoulder structure ($\Delta\omega=0.29$ eV) for the IR envelope reconstruction is however limited due to possible contamination from higher vibrational transitions in molecules as it will be discussed in next sections.

III C. XTAS from IR-driven CO molecule

Now we are in the stage to discuss the formation of XTAS profile for molecular case – a pre-aligned CO molecule resonantly pumped by ultrashort x-ray pulse on C1s→π* transition (see Sec. IIB for details of the parameters). Fig. 8 shows the XTAS obtained without IR control radiation, where the result of calculation using the full molecular description of Eqs. (1-7) is compared against the sum of the individual vibrational components $f_{0v}^{IF}S_{0v}(\omega)$ (v=0,1,2) obtained from the two-level model calculations in Eqs. (9-11). According to the computed Frank-Condon factors f_{00}^{IF}=0.874, f_{01}^{IF}=0.112 and f_{02}^{IF}=0.012, only two lowest vibrational levels of the core-excited electronic state give a sufficient contribution to the absorption profile. Note that the profile $S(\omega)$, computed as full solution for the molecular system, and the sum of the vibrational

contributions $\sum_v f_{0v}^{IF} S_{0v}(\omega)$, computed in the two-level approximation, are fully overlapped, justifying the used approximation. The profile of each vibrational component $S_{0v}(\omega)$ without the IR field shows the same character as discussed above for the two-level system (see Fig. 2b). The emission valley around 287.26 eV are mainly due to the transition $|0\rangle_I \to |0\rangle_F$, while the contribution from the transitions $|0\rangle_I \to |v=1,2\rangle_F$ is about 8%, and the others transitions are negligibly small. The main peak around 287.40 eV is not a pure absorption peak: though it is dominated by the absorption transition $|0\rangle_I \to |0\rangle_F$ the minor reduction of about 1% is due to the emission on transition $|1\rangle_F \to |1\rangle_I$, which becomes negligibly small for the photon energy above ~287.6 eV. The absorption peaks at 287.65 eV and 287.91 eV are from transitions $|0\rangle_I \to |1\rangle_F$ and $|0\rangle_I \to |2\rangle_F$, respectively. The FC factor for the transition to the second vibrational level of the core-excited state f_{02}^{IF} is rather small resulting in insignificant intensity of the absorption peak at 287.91 eV.

Fig. 9 shows XTAS of CO modified by IR field with the typical parameters ω_{IR} =0.3 eV and $\Delta\Omega_{IR}$ =0.1 eV and with respect to different values of the phase φ_{IR} . The sum of partial vibrational contributions $\sum_v f_{0v}^{IF} S_{0v}(\omega)$ and the total XTAS molecular profile $S(\omega)$ are almost coincident. In the present case the partial vibrational contributions cannot be easily separated as in the IR-free case, since the IR-induced features of one vibrational component (v=0) overlap with the main peaks of another vibrational component (v=1). The most significant IR-induced features arise around photon energy 287.10 eV and 287.70 eV. General phase φ_{IR} dependence of these shoulder structures has been comprehensively discussed for the case of two-level model (Figs. 5-6). With the help of the vibrationally separated XTAS profiles $f_{0v}^{IF} S_{0v}(\omega)$ (v=0,1,2) , all the main features can be carefully identified. The left shoulder structure at 287.1 eV is solely contributed by the transition $|0\rangle_I \to |0\rangle_F$, which allows to clearly identify its relative phase φ_{IR} dependence in the experiment, while the right shoulder structure is contaminated by the main absorption peak at 287.65 eV on the transition $|0\rangle_I \to |1\rangle_F$. Incoherent sum of these two contributions produces the peak near 287.70 eV. The main absorption peak around 287.40 eV is dominating and the relatively

small contribution from the left shoulder of the transition $|0\rangle_I \rightarrow |1\rangle_F$ is not visible in the total profile. The peak around 287.91 eV appearing from transition $|0\rangle_I \rightarrow |2\rangle_F$ has rather small intensity giving a tiny contribution to the total profile. It is worthwhile to note, that the IR field frequency in the present case is rather similar to the vibrational frequency of the core-excited state ~0.26 eV [45], which results in partial overlap between the IR-induced shoulder structures and the main vibrational peaks, sufficiently modifying the core-excited wave packet dynamics monitored by the XTAS. A change of the IR frequency can separate spectrally the contribution of conventional vibrational structure from the IR field induced structures. Moreover, the IR-induced structure in the left shoulder of the main absorption peak of the lowest vibrational level (~287.10 eV) is free from the other vibrational contributions. Due to this, for the first possible experimental observation of the dynamic Stark effect in XTAS, described in the present paper, the measurements of the XTAS profile below the resonance with the frequency detuning equals to frequency of the IR field is advised. As discussed above (Sec. III C), this effect can be used for the fine tuning and phase synchronization between the CW IR field and an x-ray pulse, which is highly demanded in various modern x-ray non-linear applications.

III D. XTAS on oxygen K-edge of CO

The x-ray absorption spectra of CO molecule on carbon K-edge is dominated by the lowest vibrational transition $|0\rangle_I \rightarrow |0\rangle_F$, which makes the two-level scheme a robust approximation. In a general case many vibrational transitions can give contribution and to overlap with each other breaking down the two-level approximation. Such situation is happened at O1s→π* core-excitation in CO molecule analyzed in Fig. 10. Due to a large shift of the equilibrium internuclear distance of the core-excited state as compared to the ground state, the conventional x-ray absorption profile is strongly broadened due to vibrational excitation with the maximum corresponding to the $|0\rangle_I \rightarrow |4\rangle_F$ transition [45]. Moreover, larger lifetime broadening at oxygen K-edge (Γ_F =0.18 eV) and a smaller vibration frequency of the core-excited potential 0.18 eV results in much stronger LVI effect as compared to the case of carbon K-edge excitation. Due to this the two-level model cannot be used as a valid approximation in the present case.

The XTAS profile without IR field is shown in Fig. 10a, where the positions of the two

lowest vibrational levels are shown with dashed vertical lines. The deep emission valley of XTAS near 533.2 eV is formed by contribution of many vibrational transitions and these contributions cannot be separated in the present case due to strong overlap and LVI. The IR-field effects can be obviously observed by comparison of the two profiles in Fig. 10a. The left IR-induced shoulder structures of the vibrational transitions $|0\rangle_I \to |0\rangle_F$ and $|0\rangle_I \to |1\rangle_F$, whose positions are shown by the dashed lines, clearly give a sufficient contribution to the XTAS profile. Variation of the IR phase, as it is illustrated in Fig. 10b, results in drastic change of the XTAS profile. In particularly, the deep valley at 533.2 eV observed in the IR-field free case and IR-field with phase $\varphi_{IR} = \pi$ (Fig. 10a) is completely quenched when the phase of IR-field equals to 0 (black curve in Fig. 10b). Such a strong modification of the XTAS profile is the result of collective contribution from several vibrational transition and their interference. Although it is impossible to isolate a shoulder structure corresponding to the individual vibrational transition in the present, the total XTAS profile shows strong dependence on the IR phase and thus, in principle, also can be used for the fine phase synchronization with ultrashort x-ray pulse.

IV. Conclusions

A scheme of x-ray transient absorption spectra for pre-aligned molecules by implementing a femtosecond x-ray pump and CW IR-control scenario is investigated using CO molecule as a prototype. CO is resonantly pumped into carbon- and oxygen-edge core-excited 1s→π^* states by a weak femtosecond x-ray pulse, simultaneously, IR-control radiation induces dynamic Stark shifts on the ground and core-excited states and modulating the wave packet dynamics. It is shown that the dynamic Stark effect contributes significantly to XTAS forming shoulder structures of the main absorption resonance; these structures can be efficiently manipulated by varying the time delay or relative phase between IR field and x-ray pulse. Large energy separation between the IR-control and x-ray pump photons used in the proposed scheme allows to observe clearly dynamic Stark effect free from multiphoton contribution, nonlinear, and off-resonant effects. A simple two-level model system is constructed to identify and interpret the emission and absorption structures appearing in the complex XTAS. In this framework the total spectra can be efficiently decomposed as incoherent sum of the profiles of different vibrational components obtained from

the simple two-level model and weighted by the Frank-Condon factors, providing deeper insight in the IR-induced XTAS features. Due to its high sensitivity to the IR frequency and phase, the predicted effect can be used for controlled manipulation of the nuclear dynamics in molecules, as well as for the fine phase synchronization of the x-ray pulse to the 'comb' of the IR field, required in various modern applications of ultrashort x-ray free-electron laser pulses.

Acknowledgements

Grants from the National Basic Research Program of China (2017YFA0403200), NSFC (11604197), the Science Challenge Program of China (TZ2018005 and TZ2016005), and the Organization Department of CCCPC are acknowledged. VK acknowledges financial support from Swedish Research Council (VR) and within the State Contract of the Ministry of Education and Science of the Russian Federation for Siberian Federal University for Scientific Research in 2017–2019 Project 3.2662.2017.

References:

[1] S. Bengtsson, E. W. Larsen, D. Kroon, S. Camp, M. Miranda, C. L. Arnold, A. L'Huillier, K. J. Schafer, M. B. Gaarde, L. Rippe *et al.*, Nat. Photonics **11**, 252 (2017).

[2] F. Calegari, G. Sansone, S. Stagira, C. Vozzi, and M. Nisoli, J. Phys. B: At., Mol. Opt. Phys. **49**, 062001 (2016).

[3] P. B. Corkum and F. Krausz, Nat. Phys. **3**, 381 (2007).

[4] L. Gallmann, C. Cirelli, and U. Keller, Annu. Rev. Phys. Chem. **63**, 447 (2012).

[5] J. E. Bækhøj, C. Lévêque, and L. B. Madsen, Phys. Rev. Lett. **121**, 023203 (2018).

[6] J. E. Bækhøj, L. Yue, and L. B. Madsen, Phys. Rev. A **91**, 043408 (2015).

[7] Y. Cheng, M. Chini, X. Wang, A. González-Castrillo, A. Palacios, L. Argenti, F. Martín, and Z. Chang, Phys. Rev. A **94**, 023403 (2016).

[8] M. Holler, F. Schapper, L. Gallmann, and U. Keller, Phys. Rev. Lett. **106**, 123601 (2011).

[9] Y. Kobayashi, H. Timmers, M. Sabbar, S. R. Leone, and D. M. Neumark, Phys. Rev. A **95**, 031401 (2017).

[10] C. Ott, A. Kaldun, L. Argenti, P. Raith, K. Meyer, M. Laux, Y. Zhang, A. Blättermann, S. Hagstotz, T. Ding *et al.*, Nature **516**, 374 (2014).

[11] S. Pabst, A. Sytcheva, A. Moulet, A. Wirth, E. Goulielmakis, and R. Santra, Phys. Rev. A **86**, 063411 (2012).

[12] M. Sabbar, H. Timmers, Y.-J. Chen, A. K. Pymer, Z.-H. Loh, Scott G. Sayres, S. Pabst, R. Santra, and S. R. Leone, Nat. Phys. **13**, 472 (2017).

[13] H. Wang, M. Chini, S. Chen, C.-H. Zhang, F. He, Y. Cheng, Y. Wu, U. Thumm, and Z. Chang, Phys. Rev. Lett. **105**, 143002 (2010).

[14] E. R. Warrick, W. Cao, D. M. Neumark, and S. R. Leone, J. Phys. Chem. A **120**, 3165 (2016).

[15] E. R. Warrick, J. E. Bækhøj, W. Cao, A. P. Fidler, F. Jensen, L. B. Madsen, S. R. Leone, and D. M.

Neumark, Chem. Phys. Lett. **683**, 408 (2017).
[16] J. J. Rørstad, N. S. Ravn, L. Yue, and L. B. Madsen, Phys. Rev. A **98**, 053401 (2018).
[17] C.-T. Liao, X. Li, D. J. Haxton, T. N. Rescigno, R. R. Lucchese, C. W. McCurdy, and A. Sandhu, Phy. Rev. A **95**, 043427 (2017).
[18] Y. He, Z. Liu, Z. Cui, Y. Zhang, A. N. Pfeiffer, T. Pfeifer, J. Ding, and B. Hu, Phys. Rev. A **99**, 053418 (2019).
[19] A. Wirth, M. T. Hassan, I. Grguraš, J. Gagnon, A. Moulet, T. T. Luu, S. Pabst, R. Santra, Z. A. Alahmed, A. M. Azzeer *et al.*, Science **334**, 195 (2011).
[20] M. Hollstein, R. Santra, and D. Pfannkuche, Phys. Rev. A **95**, 053411 (2017).
[21] M. X. Wu, S. H. Chen, S. Camp, K. J. Schafer, and M. B. Gaarde, Journal of Physics B-Atomic Molecular and Optical Physics **49**, 062003 (2016).
[22] M. Schultze, K. Ramasesha, C. D. Pemmaraju, S. A. Sato, D. Whitmore, A. Gandman, J. S. Prell, L. J. Borja, D. Prendergast, K. Yabana *et al.*, Science **346**, 1348 (2014).
[23] C.-T. Liao, A. Sandhu, S. Camp, K. J. Schafer, and M. B. Gaarde, Phys. Rev. Lett. **114**, 143002 (2015).
[24] C.-T. Liao, X. Li, D. J. Haxton, T. N. Rescigno, R. R. Lucchese, C. W. McCurdy, and A. Sandhu, Phys. Rev. A **95**, 043427 (2017).
[25] S. B. Zhang, V. Kimberg, and N. Rohringer, Phys. Rev. A **94**, 063413 (2016).
[26] Y. Pertot, C. Schmidt, M. Matthews, A. Chauvet, M. Huppert, V. Svoboda, A. von Conta, A. Tehlar, D. Baykusheva, J.-P. Wolf *et al.*, Science **355**, 264 (2017).
[27] A. R. Attar, A. Bhattacherjee, C. D. Pemmaraju, K. Schnorr, K. D. Closser, D. Prendergast, and S. R. Leone, Science **356**, 54 (2017).
[28] A. Chew, N. Douguet, C. Cariker, J. Li, E. Lindroth, X. Ren, Y. Yin, L. Argenti, W. T. Hill, and Z. Chang, Phys. Rev. A **97**, 031407 (2018).
[29] C. Bostedt, S. Boutet, D. M. Fritz, Z. Huang, H. J. Lee, H. T. Lemke, A. Robert, W. F. Schlotter, J. J. Turner, and G. J. Williams, Rev. Mod. Phys. **88**, 015007 (2016).
[30] K. Tiedtke, A. Azima, N. von Bargen, L. Bittner, S. Bonfigt, S. Düsterer, B. Faatz, U. Frühling, M. Gensch, C. Gerth *et al.*, New J. Phys. **11**, 023029 (2009).
[31] E. Allaria, C. Callegari, D. Cocco, W. M. Fawley, M. Kiskinova, C. Masciovecchio, and F. Parmigiani, New J. Phys. **12**, 075002 (2010).
[32] J. Li, X. Ren, Y. Yin, K. Zhao, A. Chew, Y. Cheng, E. Cunningham, Y. Wang, S. Hu, Y. Wu *et al.*, Nat. Commun. **8**, 186 (2017).
[33] K. Zhao, Q. Zhang, M. Chini, Y. Wu, X. Wang, and Z. Chang, Opt. Lett. **37**, 3891 (2012).
[34] T. Gaumnitz, A. Jain, Y. Pertot, M. Huppert, I. Jordan, F. Ardana-Lamas, and H. J. Wörner, Opt. Express **25**, 27506 (2017).
[35] W. Helml, A. R. Maier, W. Schweinberger, I. Grguraš, P. Radcliffe, G. Doumy, C. Roedig, J. Gagnon, M. Messerschmidt, S. Schorb *et al.*, Nat. Photonics **8**, 950 (2014).
[36] K. C. Prince, E. Allaria, C. Callegari, R. Cucini, G. De Ninno, S. Di Mitri, B. Diviacco, E. Ferrari, P. Finetti, D. Gauthier *et al.*, Nat. Photonics **10**, 176 (2016).
[37] N. Hartmann, W. Helml, A. Galler, M. R. Bionta, J. Grünert, S. L. Molodtsov, K. R. Ferguson, S. Schorb, M. L. Swiggers, and S. Carron, Nat. Photonics **8**, 706 (2014).
[38] L. S. Cederbaum, Y.-C. Chiang, P. V. Demekhin, and N. Moiseyev, Phys. Rev. Lett. **106**, 123001 (2011).
[39] P. V. Demekhin, Y.-C. Chiang, and L. S. Cederbaum, Phys. Rev. A **84**, 033417 (2011).

[40] L. X. Chen and X. Zhang, J. Phys. Chem. Lett. **4**, 4000 (2013).
[41] L. X. Chen, X. Zhang, and M. L. Shelby, Chem. Sci. **5**, 4136 (2014).
[42] M. B. Gaarde, C. Buth, J. L. Tate, and K. J. Schafer, Phys. Rev. A **83**, 013419 (2011).
[43] X. Li, B. Bernhardt, A. R. Beck, E. R. Warrick, A. N. Pfeiffer, M. Justine Bell, D. J. Haxton, C. William McCurdy, D. M. Neumark, and S. R. Leone, J. Phys. B: At., Mol. Opt. Phys. **48**, 125601 (2015).
[44] E. Pahl, H. D. Meyer, and L. S. Cederbaum, Z. Phys. D: At., Mol. Clusters **38**, 215 (1996).
[45] P. Skytt, P. Glans, K. Gunnelin, J. Guo, and J. Nordgren, Phys. Rev. A **55**, 146 (1997).
[46] B. Wolter, M. G. Pullen, M. Baudisch, M. Sclafani, M. Hemmer, A. Senftleben, C. D. Schröter, J. Ullrich, R. Moshammer, and J. Biegert, Phys. Rev. X **5**, 021034 (2015).
[47] L. von Grafenstein, M. Bock, D. Ueberschaer, K. Zawilski, P. Schunemann, U. Griebner, and T. Elsaesser, Opt. Lett. **42**, 3796 (2017).
[48] G. A. Worth, H. D. Meyer, H. Köppel, L. S. Cederbaum, and I. Burghardt, Int. Rev. Phys. Chem. **27**, 569 (2008).
[49] M. H. Beck, A. Jackle, G. A. Worth, and H. D. Meyer, Phys. Rep. **324**, 1 (2000).
[50] J. J. Rørstad, N. S. W. Ravn, L. Yue, and L. B. Madsen, Phys. Rev. A **98**, 053401 (2018).
[51] U. Fano, Phys. Rev. **124**, 1866 (1961).
[52] U. Fano and J. W. Cooper, Phys. Rev. **137**, A1364 (1965).
[53] S. B. Zhang, X. T. Xie, and J. G. Wang, Phys. Rev. A **96**, 053420 (2017).
[54] M. O. Krause and J. H. Oliver, J. Phys. Chem. Ref. Data **8**, 329 (1979).
[55] F. F. Guimaraes, V. Kimberg, V. C. Felicissimo, F. Gel'mukhanov, A. Cesar, and H. Ågren, Phys. Rev. A **71**, 043407 (2005).
[56] N. Ignatova, V. V. Cruz, R. C. Couto, E. Ertan, A. Zimin, F. F. Guimaraes, S. Polyutov, H. Agren, V. Kimberg, M. Odelius *et al.*, Sci. Rep. **7**, 43891 (2017).
[57] A. Marinelli, R. Coffee, S. Vetter, P. Hering, G. West, S. Gilevich, A. Lutman, S. Li, T. Maxwell, and J. Galayda, Phys. Rev. Lett. **116**, 254801 (2016).

Figure captions

Figure 1. (Color online) Schematic representation of x-ray pump (ω_{xfel}) and CW-IR control (ω_{IR}) scenario; the IR pulse phase φ_{IR} relative to the peak intensity of the pump pulse (centered at t_0 =10 fs) is shown (b); pre-aligned CO molecule is resonantly pumped by the ultrashort x-ray pulse from the ground $\left|\mathrm{X}\,^1\Sigma^+\right\rangle$ into $\left|\mathrm{C}1s^{-1}\pi^*\,^1\Pi\right\rangle$ core-excited state with decay rate Γ_F , simultaneously, CW IR radiation induces dynamic stark shifts on the both electronic states, giving rise to x-ray transient absorption spectra studied here (a); two-level simplified model is presented to reveal the vibrational contributions of the molecular spectra (c). Please refer to the text for details of the models. The molecular parameters in plot (a) are taken from Ref. [45].

Figure 2. (Color online) (a) Shown are the XTAS with respect to the relative photon energy $\Delta\omega = \omega - \omega_{xfel}$ of the two-level model system for different energy detuning of the ultrashort (τ =2 fs) weak x-ray pump pulse from the resonance $\Delta = \Delta E_{00}^{FI} - \omega_{xfel}$. The decay rate of the core-excited state Γ_F =0.1 eV, IR frequency ω_{IR} =0.3 eV, relative Rabi frequency $\Delta\Omega_{IR}$ =0.1 eV and the phase of the IR field φ_{IR} =0 relative to the maximum of the envelope of x-ray pump pulse centered at t_0 =10 fs. (b) The same as (a) but with IR field is turned off $\Delta\Omega_{IR}$ =0.

Figure 3. (Color online) XTAS profile in the two-level model simulations for the resonant case (Δ =0) with variation of the decay rate Γ_F from 0.05 to 0.3 eV and relative Rabi frequency $\Delta\Omega_{IR}$ =0.2, 0.1, and 0.0 eV in the plots (a), (b) and (c), respectively. The other parameters are the same as in Fig. 2.

Figure 4. (Color online) (a) XTAS profile for the two-level system for the resonant case (Δ =0) with IR frequency ω_{IR} varying from 0.1 to 0.5 eV and relative Rabi frequency $\Delta\Omega_{IR}$ =0.1 eV; (b) time dependence of the real part of the induced wave packet $\mathrm{Re}\left[c_v^F(t)\right]$. The other parameters are the same as in Fig. 2.

Figure 5. (Color online) (a) 2D XTAS map with respect to the changes of the relative phase

difference φ_{IR} in the two-level model system for the resonant case (Δ=0); the other parameters are as in Fig. 2. The vertical dashed line shows a cut of the 2D map at $\Delta\omega$=-0.29 eV – maximum of the left-sided IR-induced structure (Figs. 6-7).

Figure 6. (Color online) XTAS profile (a) and the real part of the induced wave packet (b) with phase φ_{IR} varying from 0 to 2π, ω_{IR}=0.3 eV. The spectra in panel (a) are the horizontal cuts of 2D plot of Fig. 5 at corresponding values of the phase φ_{IR}.

Figure 7. Schematics of the dynamic Stark effect in XTAS applied for the mapping of the IR electric field envelope and IR-phase synchronization with the peak of ultrashort x-ray pulse. (a) The phase dependence of the peak maximum of IR-induced shoulder structure in XTAS at $\Delta\omega$ =-0.29 eV (Fig. 5). (b) Time dependence of the IR electric field $\varepsilon_{IR}(t) \propto \cos[\omega_{IR}(t-t_0)+\varphi_{IR}]$ (ω_{IR} =0.3 eV) with period $T_{IR} = 2\pi / \omega_{IR}$ and the real part of the core-excited wave packet $\mathrm{Re}\left[c_v^F(t)\right]$ for ultrashort x-ray pulse (τ=0.2 fs) centered at t_0 and t_d=t_0+ $2T_{IR}/3$. The estimated ultrashort x-ray pulses are also shown as shaded areas at time of t_0 and t_d.

Figure 8. (Color online) Carbon K-edge XTAS of pre-aligned CO molecule resonantly pumped by the x-ray pulse of τ=2 fs and ω_{xfel}=287.40 eV, the IR field is turned off. Contribution of different vibrational transitions $|0\rangle_I \rightarrow |v\rangle_F, v = 0,1,2$ are singled out. The sum of the vibrational contributions and the total XTAS profile computed with the full solution of the molecular system using Eq. (5) are fully overlapped.

Figure 9. (Color online) Same as in Fig. 8, but in presence of CW IR field with typical parameters ω_{IR}=0.3 eV and $\Delta\Omega_{IR}$=0.1 eV. The effect of the IR phase φ_{IR} change is illustrated through plots (a-f).

Figure 10. (Color online) XTAS on OK-edge excitation of pre-aligned CO molecule with IR field ω_{IR}=0.3 eV and $\Delta\Omega_{IR}$=0.3 eV. (a) The formation of the deep XTAS valley in IR field free case and the case of $\varphi_{IR} = \pi$; (b) dependence of XTAS profile on the IR phase variation.

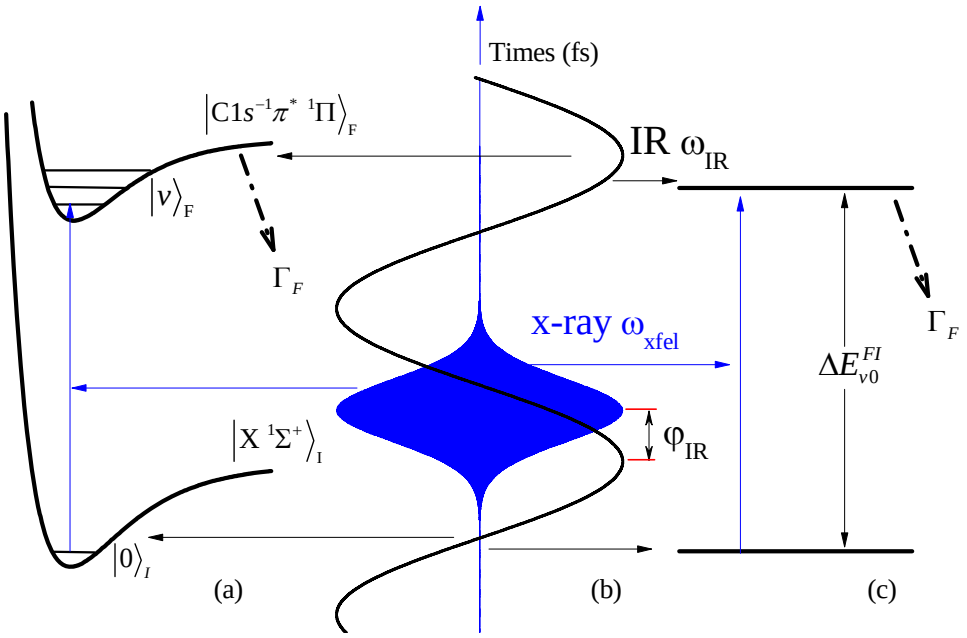
Times (fs)
$|C1s^{-1}\pi^{*}\ ^{1}\Pi\rangle_F$
IR ω_{IR}
$|v\rangle_F$
Γ_F
x-ray ω_{xfel}
Γ_F
ΔE_{v0}^{FI}
$|X\ ^{1}\Sigma^{+}\rangle_I$
φ_{IR}
$|0\rangle_I$
(a)
(b)
(c)

Fig. 1

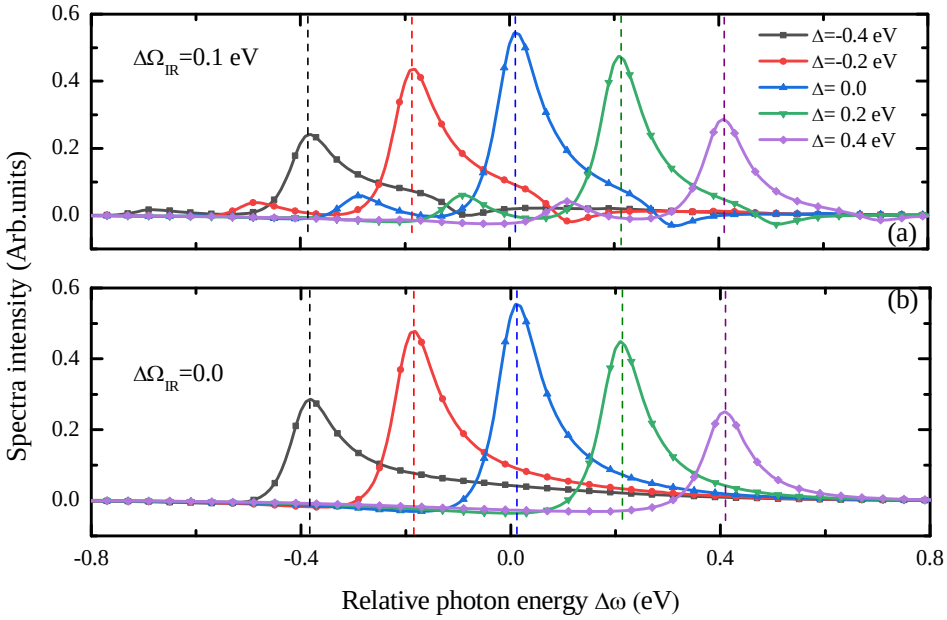
$\Delta\Omega_{IR}$=0.1 eV
Δ=-0.4 eV
Δ=-0.2 eV
Δ= 0.0
Δ= 0.2 eV
Δ= 0.4 eV
(a)
(b)
$\Delta\Omega_{IR}$=0.0
Spectra intensity (Arb.units)
Relative photon energy Δω (eV)
0.6
0.4
0.2
0.0
-0.8
-0.4
0.0
0.4
0.8

Fig. 2

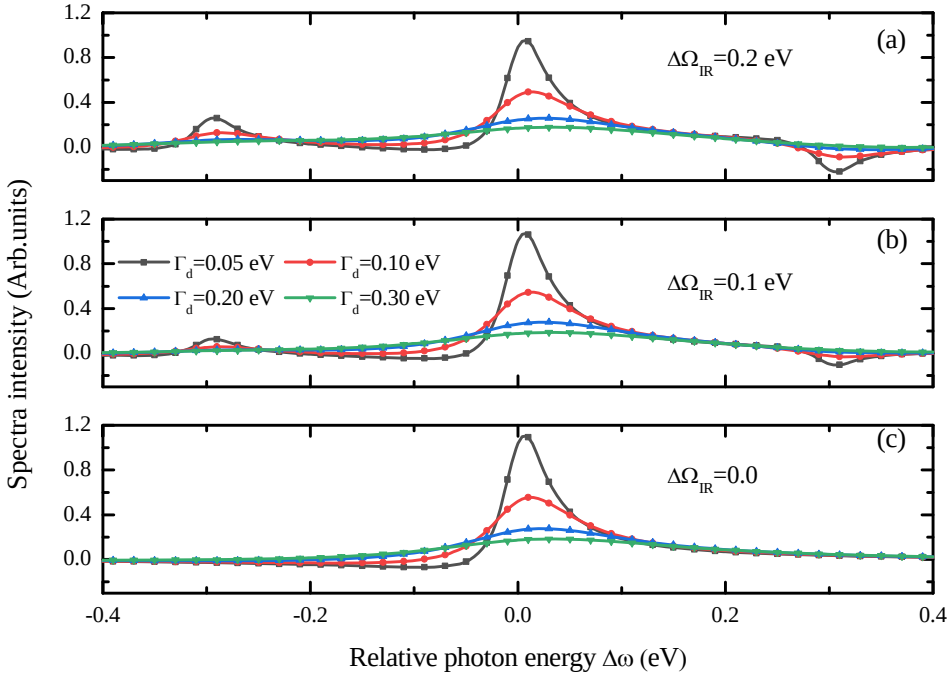
(a)
ΔΩIR=0.2 eV
(b)
Γd=0.05 eV
Γd=0.10 eV
Γd=0.20 eV
Γd=0.30 eV
ΔΩIR=0.1 eV
(c)
ΔΩIR=0.0
Spectra intensity (Arb.units)
Relative photon energy Δω (eV)

Fig. 3

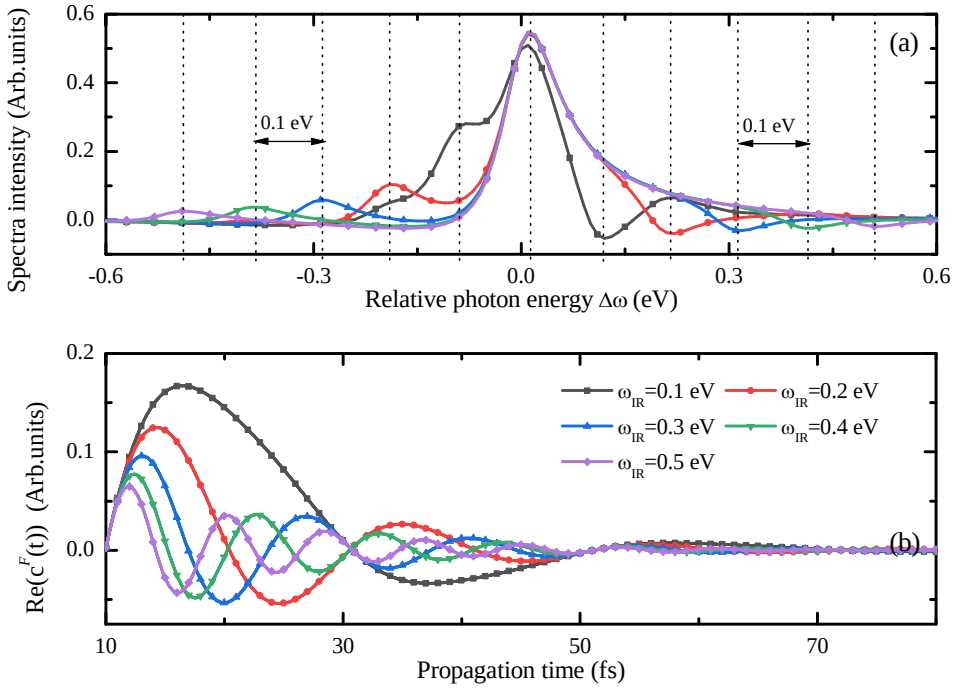
(a)
0.1 eV
0.1 eV
Spectra intensity (Arb.units)
Relative photon energy Δω (eV)
ωIR=0.1 eV
ωIR=0.2 eV
ωIR=0.3 eV
ωIR=0.4 eV
ωIR=0.5 eV
(b)
Re(c^F(t)) (Arb.units)
Propagation time (fs)

Fig. 4

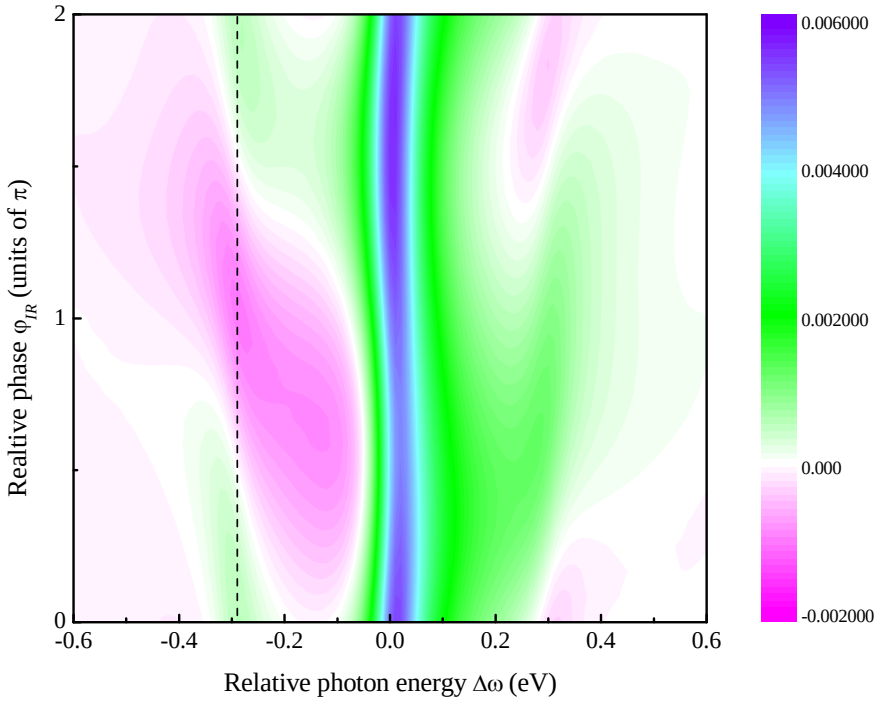
Realtive phase φ_{IR} (units of π)
Relative photon energy Δω (eV)
0.006000
0.004000
0.002000
0.000
-0.002000

Fig. 5

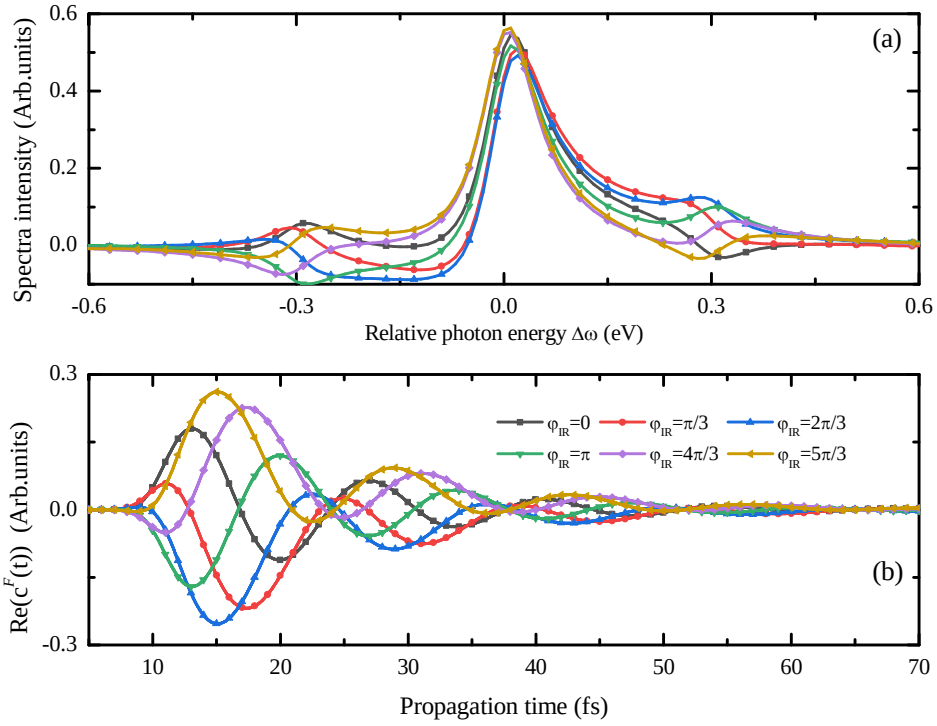
Spectra intensity (Arb.units)
Relative photon energy Δω (eV)
(a)
Re(c^F(t)) (Arb.units)
Propagation time (fs)
φ_{IR}=0
φ_{IR}=π/3
φ_{IR}=2π/3
φ_{IR}=π
φ_{IR}=4π/3
φ_{IR}=5π/3
(b)

Fig. 6

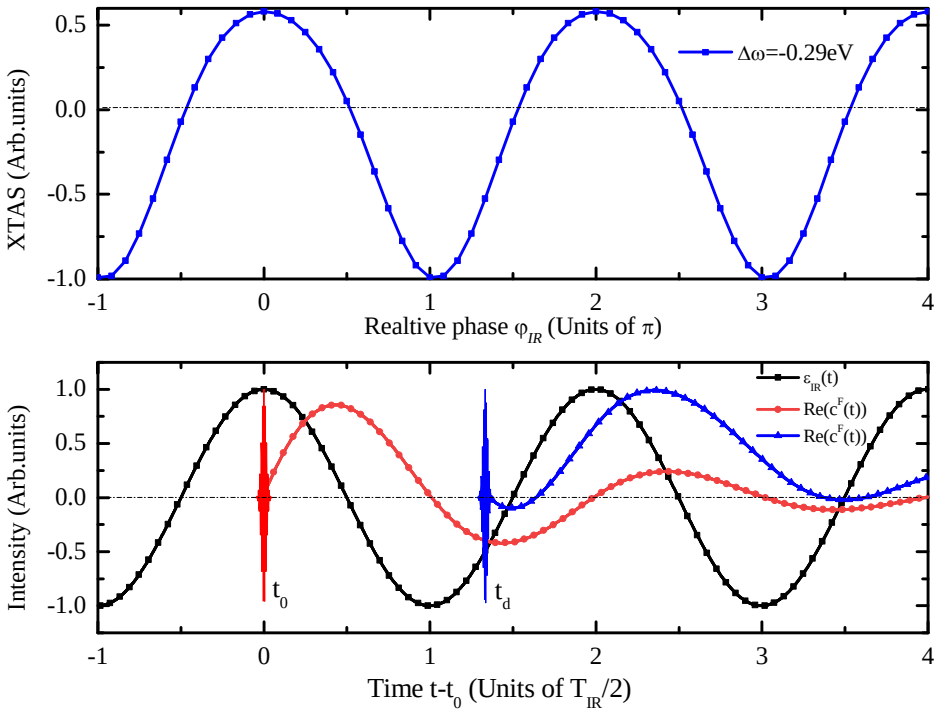
XTAS (Arb.units)
Δω=-0.29eV
Realtive phase φ_IR (Units of π)
Intensity (Arb.units)
ε_IR(t)
Re(c^F(t))
Re(c^F(t))
t_0
t_d
Time t-t_0 (Units of T_IR/2)

Fig. 7

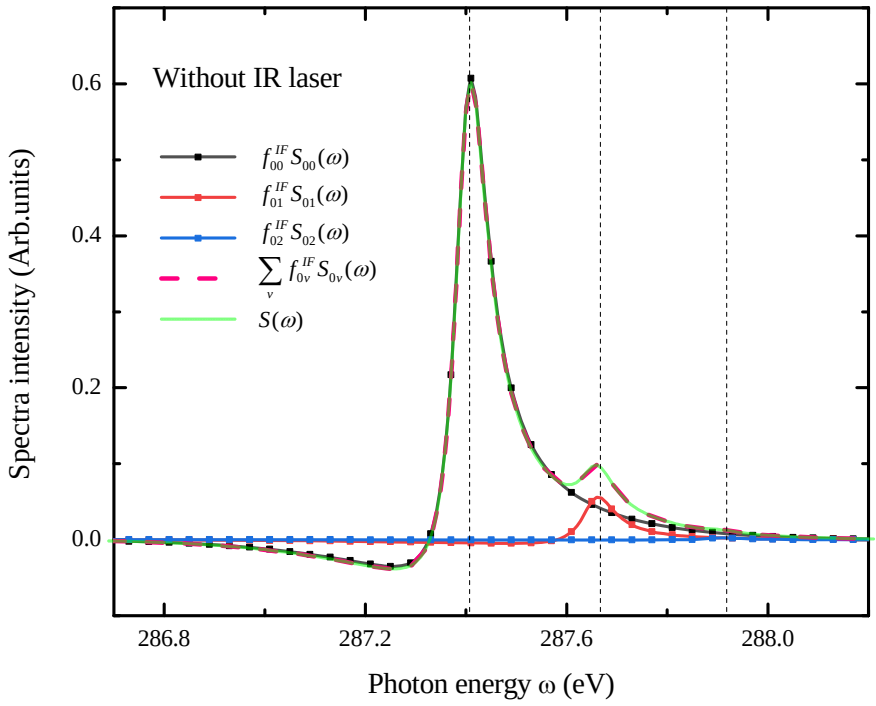
Without IR laser
$f_{00}^{IF} S_{00}(\omega)$
$f_{01}^{IF} S_{01}(\omega)$
$f_{02}^{IF} S_{02}(\omega)$
$\sum_v f_{0v}^{IF} S_{0v}(\omega)$
$S(\omega)$
Spectra intensity (Arb.units)
Photon energy ω (eV)

Fig. 8

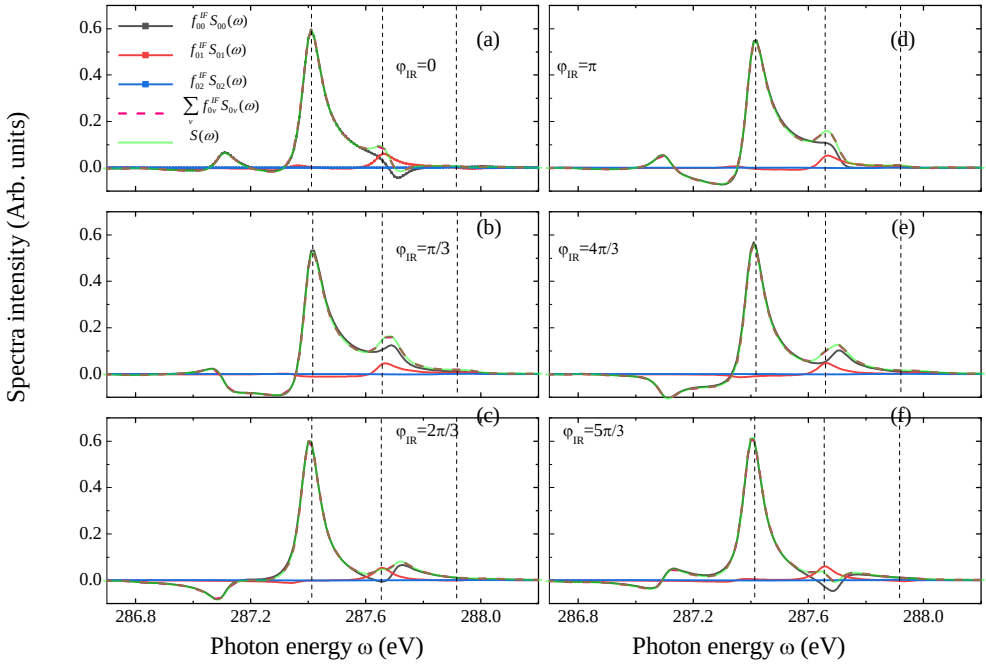

Fig. 9

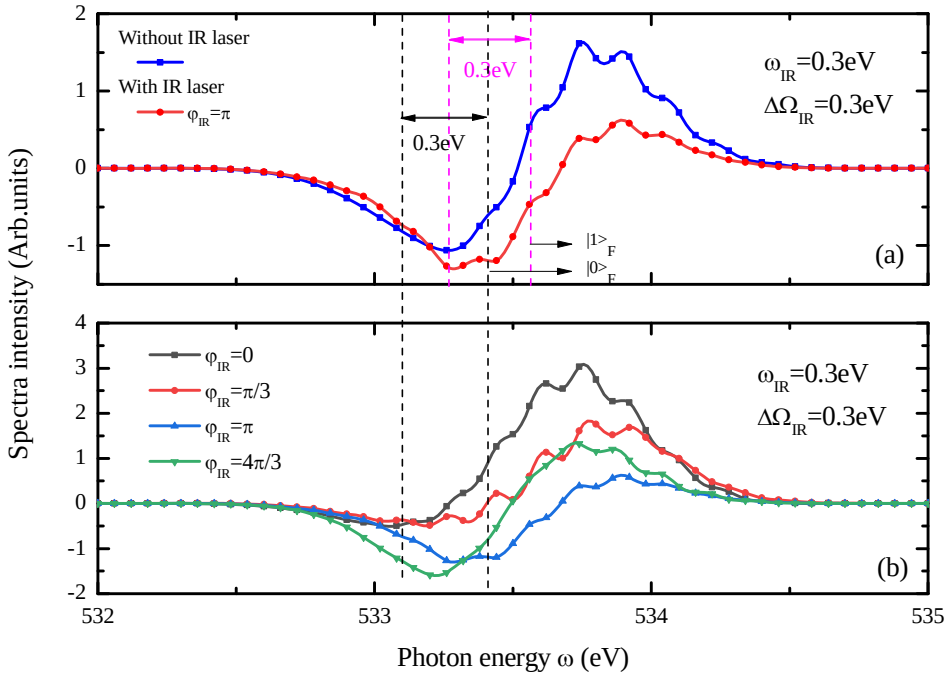

Fig. 10